Published in final edited form as:
Cell Rep. 2014 April 10; 7(1): 1–11. doi:10.1016/j.celrep.2014.03.019.

Intrinsic Membrane Hyperexcitability of ALS Patient-Derived Motor Neurons

Brian J. Wainger[1,2,*], **Evangelos Kiskinis**[3,*], **Cassidy Mellin**[1], **Ole Wiskow**[3], **Steve S.W. Han**[3,4], **Jackson Sandoe**[3], **Numa P. Perez**[1], **Luis A. Williams**[3], **Seungkyu Lee**[1], **Gabriella Boulting**[3], **James D. Berry**[4], **Robert H. Brown Jr**[5], **Merit E. Cudkowicz**[4], **Bruce P. Bean**[6], **Kevin Eggan**[3,4,7], and **Clifford J. Woolf**[1,6]

[1]FM Kirby Neurobiology Center, Boston Children's Hospital and Harvard Stem Cell Institute

[2]Department of Anesthesia, Critical Care and Pain Medicine, Massachusetts General Hospital

[3]Harvard Stem Cell Institute, Department of Stem Cell and Regenerative Biology, Harvard University and the Stanley Center for Psychiatric Research, Broad Institute

[4]Department of Neurology, Massachusetts General Hospital

[5]Department of Neurology, University of Massachusetts Medical Center

[6]Department of Neurobiology, Harvard Medical School

[7]The Howard Hughes Medical Institute, USA

SUMMARY

Amyotrophic lateral sclerosis (ALS) is a fatal neurodegenerative disease of the motor nervous system. We show using multi-electrode array and patch clamp recordings that hyperexcitability detected by clinical neurophysiological studies of ALS patients is recapitulated in induced pluripotent stem cell-derived motor neurons from ALS patients harboring superoxide dismutase 1 (*SOD1*), *C9orf72* and fused-in-sarcoma mutations. Motor neurons produced from a genetically corrected, but otherwise isogenic, $SOD1^{+/+}$ stem cell line do not display the hyperexcitability phenotype. $SOD1^{A4V/+}$ ALS patient-derived motor neurons have reduced delayed-rectifier potassium current amplitudes relative to control-derived motor neurons, a deficit that may underlie their hyperexcitability. The Kv7 channel activator retigabine both blocks the hyperexcitability and improves motor neuron survival *in vitro* when tested in *SOD1* mutant ALS cases. Therefore,

Corresponding Authors: Kevin Eggan, eggan@mcb.harvard.edu, Phone: 617 496-5611, Fax: 617 384-8234. Clifford J. Woolf, clifford.woolf@childrens.harvard.edu, Phone: 617 919-2393, Fax: 617 919-2772.
*These authors contributed equally to this work.

SUPPLEMENTAL INFORMATION
Supplemental Information for this article includes three figures and three tables.

None of the authors of this manuscript have a financial interest related to this work.

electrophysiological characterization of human stem cell-derived neurons can reveal disease-related mechanisms and identify therapeutic candidates.

INTRODUCTION

ALS is a devastating, untreatable disease of upper and lower motor neurons (Kiernan et al., 2011). The excitotoxicity neurodegeneration hypothesis posits that excessive glutamatergic synaptic activity in ALS leads to calcium overload and cell death (Cleveland and Rothstein, 2001; Pasinelli and Brown, 2006). However, nerve conduction studies evaluating axonal threshold (strength-duration time constant and recovery cycle times) in ALS patients demonstrate increased axonal membrane excitability, well away from any synapses (Bostock et al., 1995; Kanai et al., 2006; Nakata et al., 2006; Vucic and Kiernan, 2006), and the degree of hyperexcitability correlates with patient survival (Kanai et al., 2012). Increased membrane excitability may be important then as a contributor to disease, and modeling suggests that either increased persistent sodium or reduced delayed-rectifier potassium currents could be responsible for the axonal hyperexcitability (Kanai et al., 2006; Tamura et al., 2006). However, whether excitability results from autonomous changes in motor neurons cannot be determined by this technique (Fritz et al., 2013).

About 10% of ALS cases are familial, and of these, superoxide dismutase 1 (*SOD1*) mutations account for about 20%. Motor neurons from $SOD1^{G93A}$ mice, which overexpress this human mutant SOD1 protein, also show hyperexcitability (Kuo et al., 2004; Pieri et al., 2003; van Zundert et al., 2008), at least in part due to increased persistent sodium currents. Because of the distinct clinical and pathological features of *SOD*1 ALS compared to other variants (Ince et al., 2011), it is unclear if primary motor neuron hyperexcitability represents a general feature of ALS or a specific characteristic of *SOD1*-mediated disease. Hyperexcitability in motor neurons of other familial ALS etiologies, such as *C9orf72* hexanucleotide repeat expansions and fused-in-sarcoma (*FUS*) mutations, have not yet been similarly evaluated because of a lack of mouse models.

Induced pluripotent stem cell (iPSC) technology enables neurons of specific disease-relevant subtypes to be derived from disease patients and control subjects, and thereby provides an *in vitro* platform for discovering human neuron phenotypes that may reflect the individual diseases. However, the number of subject cell lines employed in studies utilizing this technique has so far been small (Sandoe and Eggan, 2013). Thus, it is currently difficult to know how consistent such findings are across large numbers of patients, and if the results represent disease-specific phenotypes or differences among cell lines. We address these issues here in two ways. First, we use a gene-targeted correction of the disease-causing *SOD1* mutation to produce otherwise isogenic stem cells bearing wild-type *SOD1* alleles (Kiskinis et al., 2014) and show that the gene correction abrogates the phenotype of ALS motor neuron hyperexcitability. Second, we demonstrate that hyperexcitability is present among motor neurons derived from eight ALS patients of three separate genetic etiologies compared to five control patients, together constituting the largest sample group to date for these types of studies. ALS-derived motor neurons have reduced delayed-rectifier voltage-gated potassium currents compared to controls. Furthermore, retigabine, an activator of Kv7

potassium channels reduces excitability to levels seen in controls. Retigabine increases the *in vitro* survival of $SOD1^{A4V/+}$ ALS motor neurons, supporting the hypotheses that motor neuron hyperexcitability may contribute to motor neuron degeneration in ALS. The hyperexcitability phenotype and blockade of firing by retigabine are present across a wide range of familial ALS patients harboring additional *SOD1* mutations, *C9orf72* repeat expansions and *FUS* mutations. An iPSC-based disease-modeling approach can validate a clinically-relevant phenotype in human motor neurons, reveal mechanisms underlying the phenotype and help evaluate actions of candidate drugs on the disease-specific phenotype.

RESULTS

Hyperexcitability of $SOD1^{A4V}$-Derived Motor Neurons Using Multi-Electrode Array Recording

We performed an initial set of electrophysiological phenotyping experiments using iPSC-derived motor neurons from two control subjects (11a, 18a) and two unrelated familial ALS patients (39b and RB9d) harboring the same aggressive $SOD1^{+/A4V}$ mutation. All iPSC lines were generated via 3-factor (*OCT4*, *SOX2*, *KLF4*) retroviral reprogramming, had a normal karyotype, and differentiated into motor neurons after robust neuralization based on dual SMAD inhibition (Chambers et al., 2009) and specification through exposure to retinoic acid and induction of sonic hedgehog signaling (Boulting et al., 2011; Kiskinis et al., 2014; Figure 1A).

We recorded spontaneous firing of iPSC-derived motor neurons using extracellular multi-electrode arrays (MEAs), whereby the action potentials of individual neurons are detected by a grid of 64 extracellular electrodes embedded in each culture well. In four separate experiments, control and *SOD1* ALS iPSC lines were cultured synchronously, differentiated into motor neurons in parallel, and plated in equal numbers on MEAs, which allowed recording of the spontaneous firing (Hanson and Landmesser, 2004) in hundreds of control and ALS patient-derived neurons per differentiation after culturing for four weeks. We observed significantly more spontaneous action potentials in $SOD1^{+/A4V}$ relative to control cultures ($p<0.05$, t-test; Figure 1B,C). Action potentials were sorted by spike morphology and timing to derive clusters corresponding to individual neurons (Figure S1) (Cohen and Kohn, 2011), and a significantly higher average mean firing rate was observed in the $SOD1^{+/A4V}$ neurons ($p<10^{-15}$, t-test; Figure 1D,E).

We performed two experiments to confirm that the hyperexcitability on the MEAs resulted from motor neurons. First, to test if the difference in spontaneous action potential firing resulted from a larger number or more active population of inhibitory neurons in control cultures, we applied GABAergic and glycinergic transmission blockers. The blockers did not increase action potential firing rates ($p=0.61$, t-test, for bicuculline; $p= 0.24$, t-test, for strychnine; Figure S2), suggesting that activity of inhibitory neurons was minimal and that the heightened spontaneous firing in the MEA recordings of ALS-derived motor neurons reflected an intrinsic increase in excitability.

Second, we inserted a *Hb9*::GFP reporter into the AAVS1 locus for iPSCs 18a and 39b (Figure S3A), allowing fluorescence-activated cell sorting (FACS) purification of GFP-

positive motor neurons for recording on the arrays (Figure S3B–C). We recorded every four days and observed that 39b *Hb9*::GFP motor neurons consistently fired more action potentials than 18a *Hb9*::GFP motor neurons over the entire time course (mixed model ANOVA F-test $p=1\times10^{-4}$ for difference between lines; post-hoc t-tests after Bonferroni correction for multiple comparisons for day 12, p=0.0055; day 16, p= 0.0030; day 20, p=0.0057; day 24, p=0.0029; day 28, p=0.015; Figure 1F). Thus, the hyperexcitability must be due to motor neurons, because only *Hb9*-positive motor neurons were plated on the arrays.

Correction of the *SOD1^{A4V}* Mutation Eliminates the Hyperexcitability Phenotype

To test if increased action potential firing was a direct effect of the *SOD1^{A4V}* mutation, we took advantage of a gene-targeted derivative of the 39b iPSC line in which the A4V-encoding mutation had been corrected to a wild-type sequence by homologous recombination, 39b-*SOD1$^{+/+}$* (abbreviated 39b-Cor; Kiskinis et al., 2014). Because substantial motor neuron death begins in ALS motor neurons after 15 days of neuronal maturation in our culture conditions (Kiskinis et al., 2014) and because the hyperexcitability phenotype in the ALS motor neurons was detectable at this early time point (Figure 1F), we compared MEA recordings of 39b and isogenic-derived 39b-Cor motor neurons at 14 days, to avoid the possibility that increased firing reflected either neuronal death or select survival of hyperexcitable neurons (Table S1). While the baseline spike rate was lower at 14 than 28 days, patient-derived 39b neurons had a higher spontaneous firing rate than neurons in which the *SOD1* mutation was corrected (p=0.01 for total rate, t-test; Figure 1G; average mean firing rate 1.30 ± 0.10 Hz for n=122 39b-Cor and 1.50 ± 0.08 Hz for n=208 39b; p<0.05, t-test). We conclude that the hyperexcitability phenotype reflects the presence of the disease-initiating mutation and precedes progressive motor neuron death.

Confirmation of ALS Motor Neuron Hyperexcitability and Mechanistic Exploration Using Whole-Cell Patch Clamp

To examine the electrophysiological properties of identified individual motor neurons, we transduced developing neurons with an *Hb9*::RFP lentiviral reporter and recorded only from RFP-positive motor neurons (Marchetto et al., 2008) using whole-cell patch clamp (Figure 2A). Both control- and *SOD1* ALS-derived motor neurons were electrically excitable. To quantify the degree of excitability, we assayed the number of action potentials fired in response to a slow ramp depolarization. The number of action potentials fired by ALS motor neurons was significantly greater than control motor neurons (p<0.05, Mann-Whitney U test; Figure 2B, upper panels, Figure 2C, upper panel). Resting membrane potential, action potential threshold (rheobase) and input resistance did not differ between ALS and control motor neurons (Table S2), indicating that excitability differences were not due to differences in electrophysiological health or baseline capacity for action potential generation.

When we compared motor neurons derived from 39b-Cor and 39b cell lines in three separate additional parallel experiments, we again observed a marked difference in the number of action potentials elicited during ramp depolarization (p<0.05, Mann-Whitney U test; Figure 2B, lower panels, Figure 2C, lower panel), demonstrating that the A4V mutation was essential for the phenotype. There was variability in the number of action potentials in motor

neurons from the same line tested across multiple differentiations, but the increased number of action potentials in ALS motor neurons relative to control motor neurons was always preserved. This result underscores the importance of performing repeated parallel differentiations in which equal numbers of control and ALS motor neurons are analyzed from each differentiation.

In addition to quantifying the electrical excitability of individual neurons, patch clamp recording enables quantitative investigation of specific currents that determine excitability. To identify electrophysiological mechanisms responsible for the increased firing of mutant motor neurons, we performed voltage-clamp experiments using *Hb9*::RFP-positive motor neurons to examine current components. As an index of excitatory and inhibitory voltage-dependent ion channels, we quantified the ratio of outward delayed-rectifier potassium current to inward transient sodium current. In four repeated differentiations of motor neurons from control and $SOD1^{+/A4V}$ iPSC lines, we observed that the ratio of delayed-rectifier potassium to transient sodium current was consistently smaller in $SOD1^{+/A4V}$ motor neurons ($p<0.001$, t-test; Figure 2D–E). The difference was driven primarily by the reduced delayed-rectifier potassium channel component, as the difference in steady-state potassium current amplitude normalized to individual cell capacitance between ALS subjects and healthy controls was significant (control 137.0 ± 14.4 pA/pF, n=23, versus ALS 94.4 ± 10.7 pA/pF, n=25; $p<0.05$, t-test) whereas the peak sodium current normalized to capacitance was not (control 190.3 ± 23.0 pA/pF, n=21, versus ALS 237 ± 21.2 pA/pF, n=23; p= 0.2, t-test). Since voltage-gated potassium channels repolarize the membrane potential back to negative values after an action potential, a decrease in such currents likely contributes to increased action potential firing in ALS motor neurons.

Correction of the disease-causing $SOD1^{+/A4V}$ mutation also increased the relative steady-state delayed-rectifier potassium current amplitude, showing that this phenotypic difference specifically resulted from the A4V mutation ($p<0.005$, t-test; Figure 2F). We found a marked reduction in delayed-rectifier current magnitude in 39b compared to 39b-Cor motor neurons ($p< 0.05$, t-test; Figure 2G) but no difference in sodium current peak amplitudes ($p=0.8$, t-test; Figure 2H). Thus, correction of the deficit in delayed-rectifier potassium current in 39b-Cor motor neurons may enable repolarization of the membrane potential back to normal hyperpolarized values and reduction of excitability to levels in wild-type motor neurons.

Retigabine Blocks Motor Neuron Hyperexcitability and Increases *in vitro* Survival of $SOD1^{A4V/+}$ ALS motor neurons

Motor neurons express many types of voltage-activated potassium channels and pharmacological dissection and quantification into distinct components is challenging. Regardless of which currents produce the hyperexcitability in diseased motor neurons, Kv7 (KCNQ) channels are attractive targets for correcting the hyperexcitability because of their activation at subthreshold voltages and subsequent powerful control of excitability (Brown and Passmore, 2009). Given this and the reduced delayed-rectifier potassium currents in ALS-derived motor neurons, we hypothesized that retigabine, a specific activator of subthreshold Kv7 currents and clinically-approved anticonvulsant (Porter et al., 2007),

might block hyperexcitability in the *SOD1*$^{+/A4V}$ motor neurons. In whole-cell patch clamp, retigabine significantly increased the minimal current step necessary for action potential generation (rheobase) by 3.6 ± 2.4 pA ($p<0.05$, Wilcoxon signed rank test; Figure 3A). Retigabine also stopped spontaneous firing of *Hb9*::RFP-positive motor neurons and hyperpolarized the resting membrane potential by 6.0 ± 2.2 mV ($p=0.001$, t-test; Figure 3B). Because these experiments were performed with blockers of glutamatergic, GABAergic, and glycinergic receptors, retigabine must have a direct effect on motor neuron excitability. We used MEA recordings to determine a dose-response for inhibition of spontaneous firing by retigabine of *SOD1*$^{+/A4V}$ ALS-derived neurons. Retigabine suppressed ALS neuron spontaneous firing with an EC_{50} of 1.5 μM (Figure 3C), a concentration consistent with its pharmacological activity as an anti-epileptic agent and similar to its EC_{50} for Kv7 channels (Wickenden et al., 2000). In line with this finding, analysis of RNA-Seq data from FACS-sorted motor neurons (Kiskinis et al., 2014) confirms expression of Kv7 channels (Table S3).

To evaluate the possibility that hyperexcitability is an upstream modulator of motor neuron degeneration in ALS, we tested if retigabine affects the survival of control and *SOD1*$^{+/A4V}$ motor neurons over 30 days in culture. As observed by Kiskinis et al. under basal conditions, the loss of *SOD1*$^{+/A4V}$ motor neurons was greater than *SOD1*$^{+/+}$ control motor neurons (Kiskinis et al., 2014). Two weeks of treatment with retigabine (1 μM) increased the number of ALS motor neurons *in vitro* by 25% ($p<10^{-4}$, t-test; Figure 3D) to levels found in controls.

To investigate how retigabine increases the survival of *SOD1*$^{A4V/+}$ ALS motor neurons, we determined whether it affects pathways suspected to contribute to motor neuron death in ALS (Robberecht and Philips, 2013). We chose to look at endoplasmic reticulum (ER) stress because of the demonstration that ER stress pathways are activated in *SOD1*$^{A4V/+}$ ALS compared to *SOD1*$^{+/+}$ motor neurons (Kiskinis et al., 2014). After two weeks of treatment with retigabine (1 μM), *XBP1* splicing was markedly decreased in retigabine compared to vehicle-treated 39b *SOD1*$^{A4V/+}$ ALS motor neurons (Figure S4A–B). In addition to reduced *XBP1* splicing, we observed a decrease in *PUMA* and increase in *EIF2B3* transcript levels, consistent with down-regulation of ER stress in response to retigabine treatment (Figure S4C).

Motor Neuron Hyperexcitability is Present in Distinct ALS Forms and is Blocked by Kv7 Activators

In order to investigate whether motor neuron hyperexcitability generalized to additional ALS variants, we performed MEA recordings of motor neurons derived from iPSC lines made from two unrelated familial ALS patients with *C9orf72* hexanucleotide repeat expansion (19f and RB8b) (Kiskinis et al., 2014), which is responsible for 40–50% of familial ALS and approximately 10% of sporadic cases (Robberecht and Philips, 2013). Motor neurons derived from these patients also showed significant hyperexcitability compared to controls in both total firing rate ($p<0.05$, t-test; Figure 4A–B) and average mean neuronal firing rate ($p<10^{-5}$, t-test; Figure 4C).

We reasoned that comparing neuronal firing properties of a large group of ALS patient and control-derived motor neurons would help evaluate the robustness of the motor neuron hyperexcitability and, together with the A4V gene correction experiments, eliminate artifacts due to cell line variation. *SOD1*-derived motor neurons (four lines from four unrelated subjects harboring three different mutations), *C9orf72*-derived motor neurons (two lines from two unrelated subjects), fused-in-sarcoma (*FUS*)-derived motor neurons (two lines from two unrelated subjects harboring two different mutations) were all hyperexcitable relative to motor neurons derived from six iPSC lines made from five individual healthy controls (ANOVA, $p < 10^{-7}$; Tukey's post-hoc tests for control vs *SOD1* $p<0.01$, control vs *C9orf72* $p<0.01$, control vs *FUS* $p<0.05$; Figure 5A). Furthermore, spontaneous action potential firing in the ALS variant-derived motor neurons was uniformly blocked by retigabine (Figure 5B). Consistent with an on-target effect of retigabine, we found that a chemically distinct but less potent Kv7 current-enhancer, flupirtine (Brown and Passmore, 2009), also blocked spontaneous motor neuron firing (Figure 5C). These results demonstrate the broad relevance of motor neuron hyperexcitability for familial ALS and its sensitivity to Kv7 agonists across iPSC lines, patients and genotypic etiologies.

DISCUSSION

Neurons derived from patient iPSCs can be used to investigate physiological changes in specific neural subtypes relevant to neurodegeneration and reveal important disease mechanisms and candidate therapeutics. We found consistent hyperexcitability in motor neurons from a broad group of familial ALS patients, whose disease-causing mutations collectively span the majority of familial ALS cases. Differential excitability of particular motor neurons has been proposed to explain the selective vulnerability of specific motor neuron pools in ALS, and our data provide a possible mechanistic basis for this hypothesis (Bae et al., 2009; Saxena and Caroni, 2011).

Motor neuron hyperexcitability may contribute, therefore, to motor neuron death, although connections between hyperexcitability and motor neuron death in other ALS variants will now require investigation. Our results are consistent with multiple studies of excitotoxicity (Cleveland and Rothstein, 2001; Fritz et al., 2013) but, potentially, not with two recent studies. One postulated that increased excitability in the *SOD1*^{G93A} mouse model may be a compensatory mechanism (Saxena et al., 2013). However, systemically-administered glutamatergic and cholinergic modulators may affect multiple neuronal types, making it difficult to assess how the findings relate to motor neuron excitability, which was not measured. A second study found decreased numbers of elicited spikes in iPSC-derived motor neurons from ALS patients with *C9orf72* repeat expansion compared to controls (Sareen et al., 2013). The differences in spike count here may reflect the longer differentiation time (66–79 days), differences in surviving neuronal populations or alterations in resting membrane potential in *C9orf72* compared to control neurons. For example, the more depolarized resting potential in *C9orf72* expansion-derived neurons could result in greater sodium channel inactivation and reduced capacity for generation of multiple action potentials – indeed depolarization-induced action potential blockade may be a late phase of progressive hyperexcitability. Mouse *SOD1*^{G93A} motor neurons show hyperexcitability even at an embryonic age (Kuo et al., 2004; Pieri et al., 2003; van Zundert

et al., 2008), and neurophysiological studies reveal increased excitability in *C9orf72* repeat expansion subjects (Williams et al., 2013) in addition to other familial and sporadic ALS cases (Blair et al., 2010; Mills and Nithi, 1997; Vucic et al., 2006; Vucic and Kiernan, 2010).

Previously, attention has focused on persistent sodium currents as a mechanism of motor neuron hyperexcitability (Kuo et al., 2005; Vucic and Kiernan, 2010), and riluzole, the only approved drug for ALS, blocks this current (Urbani and Belluzzi, 2000). Our findings suggest an additional important role of voltage-activated potassium channels. Channel compartmentalization may differ between *in vivo* and cultured-neuron systems, however, a recent immunohistochemical study of human spinal cords found decreased protein levels of a delayed-rectifier potassium channel selectively in the ventral roots of sporadic ALS but not control subjects (Shibuya et al., 2011). Mutations in voltage-gated potassium channels cause other neurodegenerative diseases (Waters et al., 2006), and oxidation of potassium channels (with consequent modulation of voltage-dependence and kinetics of channel gating) has been suggested as a broad mechanism of aging and neurodegeneration (Sesti et al., 2010). DPP6, which is involved in trafficking Kv4 voltage-gated potassium channels in CA1 hippocampal neurons, is linked to ALS (Sun et al., 2011; van Es et al., 2008). Hyper-methylation and down-regulation of potassium channel genes were observed in epigenetic analyses of post-mortem ALS patient spinal cords (Figueroa-Romero et al., 2012).

Both enhanced persistent sodium and reduced potassium currents could converge to produce hyperexcitability, and both may offer complementary pharmacological targets to control it. While our study evaluated hyperexcitability as an innate or autonomous property of motor neurons, differences in excitability may also reflect interactions between motor neurons and glia or Schwann cells (Fritz et al., 2013). Hyperexcitability has also been observed in motor neurons from a mouse model of spinal muscular atrophy (Mentis et al., 2011), and there is evidence for both cell autonomous (Gogliotti et al., 2012) and non-autonomous (Imlach et al., 2012) modulation of excitability. Interestingly, spinal muscular atrophy has also been linked to DPP6, raising the possibility of potassium channel contributions (van Es et al., 2009).

The pathways connecting disease-causing mutations and decreased potassium channel function, and between hyperexcitability and motor neuron death remain to be clarified. Calcium overload through voltage-gated calcium channels (Chan et al., 2007) and activation of ER stress (Saxena and Caroni, 2011) are possibilities. The finding that decreasing motor neuron activity reduces ER stress suggests that hyperexcitability may be upstream of the unfolded protein response, explaining at least partially how hyperexcitability may contribute to motor neuron death in ALS. Because ER stress modifiers increase motor neuron activity, a vicious cycle may result in ALS from reciprocal positive feedback between hyperactivity and ER stress (Kiskinis et al., 2014).

Despite the asymptomatic early decades typical of ALS patients, we observed a disease-specific phenotype in iPSC-derived neurons cultured for only weeks. That this property manifests so quickly in culture may reflect the absence of supporting cells and the inhibitory circuitry normally present *in vivo*. Identification of a screenable electrophysiological

phenotype that contributes to motor neuron death and manifests quickly could facilitate investigation of ALS pathophysiology and identification or validation of therapeutics for individual patients. Furthermore, the phenotype may offer a personalized medicine approach to treatment, using response of stem cell-derived neurons as a guide for individual patient treatment selection; this strategy will require motor neurons derived from large cohorts of patients for validation. Studies of motor neuron excitability can now be expanded to determine whether all forms of ALS converge onto a single mechanistic pathway. More generally, our study illustrates the potential for using iPSCs differentiated into specific disease-relevant cell types to identify disease phenotypes, novel biomarkers and potential treatments.

EXPERIMENTAL PROCEDURES

iPSC Lines, Culture and Motor Neuron Differentiation

iPSC generation from patient fibroblasts obtained under IRB approval, characterization and motor neuron differentiation were performed as described in Kiskinis et al. (Kiskinis et al., 2014) and Figure S5, with iPSC line scoring as done previously (Bock et al., 2011). For transfection of 18a and 39b lines with a *Hb9*::GFP reporter (Figure S3), a 1kb *Hb9* promoter fragment (gift from Hynek Wichterle) controlling the expression of myristoylated GFP was inserted into a donor plasmid specific for the AAVS1 locus (Sigma). Subsequently, 2.5 million iPS cells were accutased and electroporated using the Neon transfection system (100µl tip; 1600V Voltage, 20ms Width, 1 Pulse; Life Technologies) with 2 µg of AAVS1 ZFN plasmid and 6 µg of modified AAVS1 donor plasmid. After nucleofection cells were plated on matrigel with mTeSR1 in the presence of ROCK inhibitor. After 48hrs, puromycin selection was applied and surviving clonal colonies were individually passaged and gDNA was extracted. PCR was used to confirm proper targeting of the cassette. Primer sequences are available upon request. Faithful expression of the reporter was verified using expression of the motor neuron marker Isl1 (Figure S3C).

iPSCs were maintained on culture dishes as described previously (Boulting et al., 2011) with modifications (Kiskinis et al., 2014) in a 24-day protocol based on initial neuralization with SB431542 (10 µM, Sigma Aldrich) and Dorsomorphin (1µM, Stemgent), and motor neuron patterning with RA (Sigma) and a small smoothened Agonist 1.3 (Calbiochem). For Figure 1F, FACS-purified neurons were grown on a confluent monolayer of primary cortical mouse glia prepared from P0–P2 mouse pups (as described in Boulting et al., 2011), which may increase firing rates compared to experiments without glia (Boehler et al., 2007).

MEA Recording

After 24 days of differentiation, equal numbers of control and ALS neurons were plated on poly-D-lysine/laminin coated p515A probes (Alpha Med Scientific) or M768-GLx 12-well plates (Axion BioSystems) at typical densities of 40,000–80,000/probe or well. All probes were visualized immediately before each recording session to confirm a full monolayer of cells. Initial experiments (11a, 18a, 39b, and RB9d comparison) were performed as close as possible to the time of patch recordings (4 weeks). However, because we wished to evaluate firing at a time point prior to significant motor neuron death (Kiskinis et al., 2014), we

performed subsequent experiments (39b-Cor and 39b comparison and all later experiments) at day 14 after dissociation (Table S1).

Recordings from 64 extracellular electrodes were made using a Med64 (Alpha Med Scientific) or Maestro (Axion BioSystems) MEA recording amplifier with a head stage that maintained a temperature of 37°C. For Med64 recordings, data were sampled at 20 kHz, digitized, and analyzed by spike clustering and spike extraction algorithms using Mobius software (Alpha Med Scientific) with a 2 kHz 9-pole Bessel low pass filter, 10 μV action threshold detection limit, and 30% cluster similarity radius. These standard settings were maintained for all analyses. We confirmed that we obtained similar results across a wide range of action potential threshold and cluster similarity radius settings. Correlation analysis to detect and correct for clusters detected by multiple electrodes was performed using custom Matlab software. Total action potential firing rates and mean neuronal firing frequencies were then determined and plotted. In order to record in larger replicates, we used the Axion Maestro MEA device, in a 12-well format with 64 extracellular electrodes in each well. For Maestro recordings, data were sampled at 15 kHz, digitized, and analyzed using Axion Integrated Studio software (Axion BioSystems) with a 200 Hz high pass and 2500 kHz low pass filter and an adaptive spike detection threshold set at 5.5 times the standard deviation for each electrode with 1 second binning. These standard settings were maintained for all Axion MEA recording and analysis.

For retigabine dose response curves, action potential numbers during one minute of recording in each concentration of retigabine were normalized to the initial action potential number during one minute of recording in standard extracellular saline solution. The EC50 value was determined by fitting the mean normalized data values to the Hill equation, $y = 1/((EC50/x)^{nH}+1)$ where nH is the Hill coefficient.

Patch Electrophysiology

Whole-cell patch recordings were performed on iPS-derived motor neurons identified by transduction with an *Hb9*::RFP lentivirus. Lentiviral transduction was typically performed 7–10 days before recording. Two large comparisons were performed, one consisting of 11a, 18a, 39b, and RB9d, and the second consisting of 39b-Cor and 39b. Each comparison was made from pooled data from multiple separate experiments, each consisting of synchronous and parallel iPSC culture and differentiation, embryoid body dissociation, plating and maturation of control- and ALS-derived neurons. Equal numbers of control and ALS motor neurons were recorded from each experiment. Comparison of the original four lines (11a, 18a, 39b, and RB9d) was made using four separate parallel differentiation experiments, while comparison of the isogenic correction comparison (39b-Cor and 39b) was performed using three separate parallel differentiation experiments.

For each experiment, neurons from control and ALS lines were dissociated after 24 days of differentiation and plated onto poly-d-lysine/laminin coated glass coverslips (20,000–40,000/coverslip) and allowed to mature for four weeks from start of differentiation. We chose four weeks as the best timepoint because this yielded the most homogeneous population of mature-appearing *Hb9*::RFP-positive motor neurons (at the requisite low cell density for patch clamp) with the most mature electrophysiological properties. Whole-cell

current-clamp and voltage-clamp recordings were performed using a Multiclamp 700B (Molecular Devices) at room temperature (21–23°C). Data were sampled at 20 kHz and digitized with a Digidata 1440A A/D interface and recorded using pCLAMP 10 software (Molecular Devices). Data were low-pass filtered at 2 kHz. Patch pipettes were pulled from borosilicate glass capillaries on a Sutter Instruments P-97 puller and had resistances of 2–4 MΩ. The pipette capacitance was reduced by wrapping the shank with Parafilm and compensated for using the amplifier circuitry. Series resistance was typically 5–10 MΩ, always less than 15 MΩ, and compensated by at least 80%. Neurons were excluded from analysis if holding current at −80 mV exceeded 100 pA, input resistance was less than 250 or greater than 2000 MΩ, or spikes elicited from −65 mV had peaks below 0 mV. Resting membrane potential was determined by averaging for 20s of recording, and afterwards a small holding current (typically with amplitude less than 5 pA) was used to clamp the resting membrane potential as close as possible to −65 mV. Rheobase was measured by applying 1 s steps in increments of 2.5 pA until an action potential was generated. Current ramps were elicited from an initial hyperpolarizing current of 10 pA for 1 s followed by a 210 pA/s depolarizing ramp of duration 1 s. Spikes on the ramps were counted if the peak voltage exceeded −10 mV. Action potential properties (Table S2) were determined using custom-written analysis software in Igor Pro (Wavemetrics) with DataAccess (Bruxton) for importing the files. For voltage-clamp recordings, voltages were elicited by 100-ms depolarizing steps from a holding potential of −80 mV to test potentials ranging from −80 mV to 50 mV in 10 mV increments. For the latter gene correction experiments the step length was increased to 200 ms to assay delayed-rectifier currents after more complete decay of transient potassium currents. For retigabine patch applications, resting membrane potential was recorded immediately before and 10 seconds after the application of 10 μM retigabine (in each case, membrane potential was an average of values sampled for 20 seconds). For all patch experiments, series resistance was monitored by brief −5 pA hyperpolarizing steps during current clamp recordings and by 5 mV hyperpolarizing steps during voltage clamp recordings. Electrode drift was measured at the end of each recording and was typically 1–2 mV. The extracellular solution was sodium-based and contained 135 mM NaCl, 5 mM KCl, 2 mM $CaCl_2$, 1 mM $MgCl_2$, 10 mM glucose, 10 mM HEPES 10, pH 7.4. The intracellular solution was potassium-based and contained 150 mM KCl, 2 mM $MgCl_2$, 10 mM HEPES, 4 mM MgATP, 0.3 mM NaGTP, 10 mM Na_2PhosCr, 1mM EGTA, pH 7.4. For isolation of delayed-rectifier potassium channels (Figure 2G), 300 nM TTX and 100 μM $CdCl_2$ were used to block voltage-gated sodium channels and voltage- and calcium-activated potassium channels, respectively. For isolation of voltage-gated sodium currents (Figure 2H), internal KCl was replaced by CsCl to block potassium currents and 100 μM $CdCl_2$ was used to block calcium currents.

Cell Survival and ER Stress Assays

Dissociated neurons (20k) were plated on poly-D-lysine/laminin coated 8-well chamber slides (BD Biosciences) containing a confluent monolayer of primary cortical mouse glia (Boulting et al., 2011). For survival analysis, slides were fixed at 3 and 30 days, and cultures were stained for counting. The number of ISL-positive, TUJ1-positive motor neurons (counter blinded to cell line identity) was normalized to the number on day 3 for each line. Retigabine (1 μM) or vehicle control was added from day 15 onwards. 11 total experiments

(control motor neurons) and nine total experiments (ALS motor neurons) were performed from the same four separate differentiations. ER stress experiments were performed as described in Kiskinis et al. In brief, in two separate independent biological replicates, 300 ng of RNA was used to generate cDNA, of which 2 μL and AmpliTaq Gold Polymerase (Applied Biosystems) were used for PCR amplification. The amounts of spliced and unspliced bands were quantified using Image J. Quantitative RT-PCR was performed in triplicate using the iSCRIPT kit (Biorad) for cDNA synthesis and SYBR green (Bio-Rad) labeling followed by amplification using the iCycler system (Bio-Rad).

Drugs

Drugs included retigabine (Santa Cruz Biotechnology), bicuculline, strychnine, D-AP5, CNQX, flupirtine, TTX (all from Tocris Bioscience). CsCl and $CdCl_2$ were from Sigma.

Statistical Analysis

$p<0.05$ was considered statistically significant. Comparisons were made between control and ALS populations using t-tests (two-tailed, unpaired)/ANOVA for continuous data and rank tests for non-parametric data (discrete measurements of number of spikes on ramps and rheobase). For analysis of MEA firing over time (Figure 1F), we used a mixed repeated measures ANOVA model with fixed effects of cell line and time and random effects of individual replicate. For effect of retigabine on specific cells (Figure 3A–B), paired tests were used. For effect of retigabine on survival (Figure 3D), we fitted a linear regression model with effects of retigabine treatment, cell line and their interaction. F-tests for difference between lines gave $p=0.0011$, for effect of retigabine $p=3.8\times10^{-4}$ and for effect modification ($p=0.015$). For ALS subjects, the effect of retigabine was an increase in cell count of 25.3% (SD 5.6, $p=6.4\times10^{-5}$). The effect estimate for 39b was 16.9% (SD 12.9, $p=0.03$) and for RB9d 39.9% (SD 11.3, $p=0.001$). For control subjects, the effect of retigabine was an increase in cell count of 6.1% (SD 5.1, $p=0.23$). For multiple genotype comparisons (Figure 5A), one-way ANOVA after log transformation to normalize variance and post-hoc Tukey tests were used to analyze multiple ALS variants. Error bars are SEM unless indicated.

Supplementary Material

Refer to Web version on PubMed Central for supplementary material.

Acknowledgments

We thank W. David and S. Cash for comments, suggestions, and review of the manuscript, K. Kapur for assistance with statistical analysis and K. Wainger for assistance with figures. This work was supported by NIH 5 T32 GM007592-33, Harvard NeuroDiscovery, ALS Association and American Brain Foundation Clinical Research Fellowship (B.J.W); Charles King Trust Postdoctoral Fellowship (E.K.); American Brain Foundation/ALS Association and KL2 MeRIT fellowship/Harvard Catalyst (S.S.W.H); ALS Therapy Alliance, P2ALS, Angel Fund, Pierre L. de Bourgknecht ALS Research Foundation, Al-Athel ALS Research Foundation, ALS Family Charitable Foundation and NIH/NINDS (1R01NS050557 and NINDS ARRA Award RC2-NS070-342) (R.H.B.); P2ALS, Project ALS, Target ALS, NINDS GO grant (5RC2NS069395-02), NINDS R24 (1U24NS078736-01) and HHMI (K.E.); NIH (5 R01 NS038253-10; 2 R01 NS038153-15), Target ALS and New York Stem Cell Foundation (C.J.W.).

References

Bae JS, Sawai S, Misawa S, Kanai K, Isose S, Kuwabara S. Differences in excitability properties of FDI and ADM motor axons. Muscle Nerve. 2009; 39:350–354. [PubMed: 19208410]

Blair IP, Williams KL, Warraich ST, Durnall JC, Thoeng AD, Manavis J, Blumbergs PC, Vucic S, Kiernan MC, Nicholson GA. FUS mutations in amyotrophic lateral sclerosis: clinical, pathological, neurophysiological and genetic analysis. J Neurol Neurosurg Psychiatry. 2010; 81:639–645. [PubMed: 19965854]

Bock C, Kiskinis E, Verstappen G, Gu H, Boulting G, Smith ZD, Ziller M, Croft GF, Amoroso MW, Oakley DH, Gnirke A, Eggan K, Meissner A. Reference Maps of human ES and iPS cell variation enable high-throughput characterization of pluripotent cell lines. Cell. 2011; 144:439–452. [PubMed: 21295703]

Boehler MD, Wheeler BC, Brewer GJ. Added astroglia promote greater synapse density and higher activity in neuronal networks. Neuron Glia Biol. 2007; 3:127–140. [PubMed: 18345351]

Bostock H, Sharief MK, Reid G, Murray NM. Axonal ion channel dysfunction in amyotrophic lateral sclerosis. Brain. 1995; 118 (Pt 1):217–225. [PubMed: 7534598]

Boulting GL, Kiskinis E, Croft GF, Amoroso MW, Oakley DH, Wainger BJ, Williams DJ, Kahler DJ, Yamaki M, Davidow L, Rodolfa CT, Dimos JT, Mikkilineni S, MacDermott AB, Woolf CJ, Henderson CE, Wichterle H, Eggan K. A functionally characterized test set of human induced pluripotent stem cells. Nat Biotechnol. 2011; 29:279–286. [PubMed: 21293464]

Brown DA, Passmore GM. Neural KCNQ (Kv7) channels. Br J Pharmacol. 2009; 156:1185–1195. [PubMed: 19298256]

Chambers SM, Fasano CA, Papapetrou EP, Tomishima M, Sadelain M, Studer L. Highly efficient neural conversion of human ES and iPS cells by dual inhibition of SMAD signaling. Nat Biotechnol. 2009; 27:275–280. [PubMed: 19252484]

Chan CS, Guzman JN, Ilijic E, Mercer JN, Rick C, Tkatch T, Meredith GE, Surmeier DJ. 'Rejuvenation' protects neurons in mouse models of Parkinson's disease. Nature. 2007; 447:1081–1086. [PubMed: 17558391]

Cleveland DW, Rothstein JD. From Charcot to Lou Gehrig: deciphering selective motor neuron death in ALS. Nat Rev Neurosci. 2001; 2:806–819. [PubMed: 11715057]

Cohen MR, Kohn A. Measuring and interpreting neuronal correlations. Nat Neurosci. 2011; 14:811–819. [PubMed: 21709677]

Figueroa-Romero C, Hur J, Bender DE, Delaney CE, Cataldo MD, Smith AL, Yung R, Ruden DM, Callaghan BC, Feldman EL. Identification of epigenetically altered genes in sporadic amyotrophic lateral sclerosis. PLoS One. 2012; 7:e52672. [PubMed: 23300739]

Fritz E, Izaurieta P, Weiss A, Mir FR, Rojas P, Gonzalez D, Rojas F, Brown RH Jr, Madrid R, van Zundert B. Mutant SOD1-expressing astrocytes release toxic factors that trigger motoneuron death by inducing hyperexcitability. J Neurophysiol. 2013; 109:2803–2814. [PubMed: 23486205]

Gogliotti RG, Quinlan KA, Barlow CB, Heier CR, Heckman CJ, Didonato CJ. Motor neuron rescue in spinal muscular atrophy mice demonstrates that sensory-motor defects are a consequence, not a cause, of motor neuron dysfunction. J Neurosci. 2012; 32:3818–3829. [PubMed: 22423102]

Hanson MG, Landmesser LT. Normal patterns of spontaneous activity are required for correct motor axon guidance and the expression of specific guidance molecules. Neuron. 2004; 43:687–701. [PubMed: 15339650]

Imlach WL, Beck ES, Choi BJ, Lotti F, Pellizzoni L, McCabe BD. SMN is required for sensory-motor circuit function in Drosophila. Cell. 2012; 151:427–439. [PubMed: 23063130]

Ince PG, Highley JR, Kirby J, Wharton SB, Takahashi H, Strong MJ, Shaw PJ. Molecular pathology and genetic advances in amyotrophic lateral sclerosis: an emerging molecular pathway and the significance of glial pathology. Acta Neuropathol. 2011; 122:657–671. [PubMed: 22105541]

Kanai K, Kuwabara S, Misawa S, Tamura N, Ogawara K, Nakata M, Sawai S, Hattori T, Bostock H. Altered axonal excitability properties in amyotrophic lateral sclerosis: impaired potassium channel function related to disease stage. Brain. 2006; 129:953–962. [PubMed: 16467388]

Kanai K, Shibuya K, Sato Y, Misawa S, Nasu S, Sekiguchi Y, Mitsuma S, Isose S, Fujimaki Y, Ohmori S, Koga S, Kuwabara S. Motor axonal excitability properties are strong predictors for

survival in amyotrophic lateral sclerosis. J Neurol Neurosurg Psychiatry. 2012; 83:734–738. [PubMed: 22566594]

Kiernan MC, Vucic S, Cheah BC, Turner MR, Eisen A, Hardiman O, Burrell JR, Zoing MC. Amyotrophic lateral sclerosis. Lancet. 2011; 377:942–955. [PubMed: 21296405]

Kiskinis E, Sandoe J, Williams LA, Boulting GL, Moccia R, Wainger BJ, Han S, Peng T, Thams S, Mikkilineni S, et al. Pathways disrupted in human ALS motor neurons identified through genetic correction of mutant *SOD1*. Cosubmission to Cell Stem Cell.

Kuo JJ, Schonewille M, Siddique T, Schults AN, Fu R, Bar PR, Anelli R, Heckman CJ, Kroese AB. Hyperexcitability of cultured spinal motoneurons from presymptomatic ALS mice. J Neurophysiol. 2004; 91:571–575. [PubMed: 14523070]

Kuo JJ, Siddique T, Fu R, Heckman CJ. Increased persistent Na(+) current and its effect on excitability in motoneurones cultured from mutant SOD1 mice. J Physiol. 2005; 563:843–854. [PubMed: 15649979]

Marchetto MC, Muotri AR, Mu Y, Smith AM, Cezar GG, Gage FH. Non-cell-autonomous effect of human SOD1 G37R astrocytes on motor neurons derived from human embryonic stem cells. Cell Stem Cell. 2008; 3:649–657. [PubMed: 19041781]

Mentis GZ, Blivis D, Liu W, Drobac E, Crowder ME, Kong L, Alvarez FJ, Sumner CJ, O'Donovan MJ. Early functional impairment of sensory-motor connectivity in a mouse model of spinal muscular atrophy. Neuron. 2011; 69:453–467. [PubMed: 21315257]

Mills KR, Nithi KA. Corticomotor threshold is reduced in early sporadic amyotrophic lateral sclerosis. Muscle Nerve. 1997; 20:1137–1141. [PubMed: 9270669]

Nakata M, Kuwabara S, Kanai K, Misawa S, Tamura N, Sawai S, Hattori T, Bostock H. Distal excitability changes in motor axons in amyotrophic lateral sclerosis. Clin Neurophysiol. 2006; 117:1444–1448. [PubMed: 16765084]

Pasinelli P, Brown RH. Molecular biology of amyotrophic lateral sclerosis: insights from genetics. Nat Rev Neurosci. 2006; 7:710–723. [PubMed: 16924260]

Pieri M, Albo F, Gaetti C, Spalloni A, Bengtson CP, Longone P, Cavalcanti S, Zona C. Altered excitability of motor neurons in a transgenic mouse model of familial amyotrophic lateral sclerosis. Neurosci Lett. 2003; 351:153–156. [PubMed: 14623129]

Porter RJ, Partiot A, Sachdeo R, Nohria V, Alves WM, Study G. Randomized, multicenter, dose-ranging trial of retigabine for partial-onset seizures. Neurology. 2007; 68:1197–1204. [PubMed: 17420403]

Robberecht W, Philips T. The changing scene of amyotrophic lateral sclerosis. Nat Rev Neurosci. 2013; 14:248–264. [PubMed: 23463272]

Sandoe J, Eggan K. Opportunities and challenges of pluripotent stem cell neurodegenerative disease models. Nat Neurosci. 2013; 16:780–789. [PubMed: 23799470]

Sareen D, O'Rourke JG, Meera P, Muhammad AK, Grant S, Simpkinson M, Bell S, Carmona S, Ornelas L, Sahabian A, Gendron T, Petrucelli L, Baughn M, Ravits J, Harms MB, Rigo F, Bennett CF, Otis TS, Svendsen CN, Baloh RH. Targeting RNA foci in iPSC-derived motor neurons from ALS patients with a C9ORF72 repeat expansion. Sci Transl Med. 2013; 5:208ra149.

Saxena S, Caroni P. Selective neuronal vulnerability in neurodegenerative diseases: from stressor thresholds to degeneration. Neuron. 2011; 71:35–48. [PubMed: 21745636]

Saxena S, Roselli F, Singh K, Leptien K, Julien JP, Gros-Louis F, Caroni P. Neuroprotection through excitability and mTOR required in ALS motoneurons to delay disease and extend survival. Neuron. 2013; 80:80–96. [PubMed: 24094105]

Sesti F, Liu S, Cai SQ. Oxidation of potassium channels by ROS: a general mechanism of aging and neurodegeneration? Trends Cell Biol. 2010; 20:45–51. [PubMed: 19850480]

Shibuya K, Misawa S, Arai K, Nakata M, Kanai K, Yoshiyama Y, Ito K, Isose S, Noto Y, Nasu S, Sekiguchi Y, Fujimaki Y, Ohmori S, Kitamura H, Sato Y, Kuwabara S. Markedly reduced axonal potassium channel expression in human sporadic amyotrophic lateral sclerosis: an immunohistochemical study. Exp Neurol. 2011; 232:149–153. [PubMed: 21906595]

Sun W, Maffie JK, Lin L, Petralia RS, Rudy B, Hoffman DA. DPP6 establishes the A-type K(+) current gradient critical for the regulation of dendritic excitability in CA1 hippocampal neurons. Neuron. 2011; 71:1102–1115. [PubMed: 21943606]

Tamura N, Kuwabara S, Misawa S, Kanai K, Nakata M, Sawai S, Hattori T. Increased nodal persistent Na+ currents in human neuropathy and motor neuron disease estimated by latent addition. Clin Neurophysiol. 2006; 117:2451–2458. [PubMed: 16996798]

Urbani A, Belluzzi O. Riluzole inhibits the persistent sodium current in mammalian CNS neurons. Eur J Neurosci. 2000; 12:3567–3574. [PubMed: 11029626]

van Es MA, van Vught PW, Blauw HM, Franke L, Saris CG, Van den Bosch L, de Jong SW, de Jong V, Baas F, van't Slot R, Lemmens R, Schelhaas HJ, Birve A, Sleegers K, Van Broeckhoven C, Schymick JC, Traynor BJ, Wokke JH, Wijmenga C, Robberecht W, Andersen PM, Veldink JH, Ophoff RA, van den Berg LH. Genetic variation in DPP6 is associated with susceptibility to amyotrophic lateral sclerosis. Nat Genet. 2008; 40:29–31. [PubMed: 18084291]

van Es MA, van Vught PW, van Kempen G, Blauw HM, Veldink JH, van den Berg LH. Dpp6 is associated with susceptibility to progressive spinal muscular atrophy. Neurology. 2009; 72:1184–1185. [PubMed: 19332697]

van Zundert B, Peuscher MH, Hynynen M, Chen A, Neve RL, Brown RH Jr, Constantine-Paton M, Bellingham MC. Neonatal neuronal circuitry shows hyperexcitable disturbance in a mouse model of the adult-onset neurodegenerative disease amyotrophic lateral sclerosis. J Neurosci. 2008; 28:10864–10874. [PubMed: 18945894]

Vucic S, Kiernan MC. Axonal excitability properties in amyotrophic lateral sclerosis. Clin Neurophysiol. 2006; 117:1458–1466. [PubMed: 16759905]

Vucic S, Kiernan MC. Upregulation of persistent sodium conductances in familial ALS. J Neurol Neurosurg Psychiatry. 2010; 81:222–227. [PubMed: 19726402]

Vucic S, Nicholson GA, Kiernan MC. Cortical hyperexcitability may precede the onset of familial amyotrophic lateral sclerosis. Brain. 2008; 131:1540–1550. [PubMed: 18469020]

Waters MF, Minassian NA, Stevanin G, Figueroa KP, Bannister JP, Nolte D, Mock AF, Evidente VG, Fee DB, Muller U, Durr A, Brice A, Papazian DM, Pulst SM. Mutations in voltage-gated potassium channel KCNC3 cause degenerative and developmental central nervous system phenotypes. Nat Genet. 2006; 38:447–451. [PubMed: 16501573]

Wickenden AD, Yu W, Zou A, Jegla T, Wagoner PK. Retigabine, a novel anti-convulsant, enhances activation of KCNQ2/Q3 potassium channels. Mol Pharmacol. 2000; 58:591–600. [PubMed: 10953053]

Williams KL, Fifita JA, Vucic S, Durnall JC, Kiernan MC, Blair IP, Nicholson GA. Pathophysiological insights into ALS with C9ORF72 expansions. J Neurol Neurosurg Psychiatry. 2013

HIGHLIGHTS

- iPSC-derived motor neurons from ALS patients are hyperexcitable compared to controls.
- Correction of the disease-causing mutation corrects the phenotype.
- Retigabine rescues the hyperexcitability phenotype in multiple ALS variants.
- Retigabine improves *in vitro* survival of $SOD1^{A4V/+}$ ALS motor neurons.

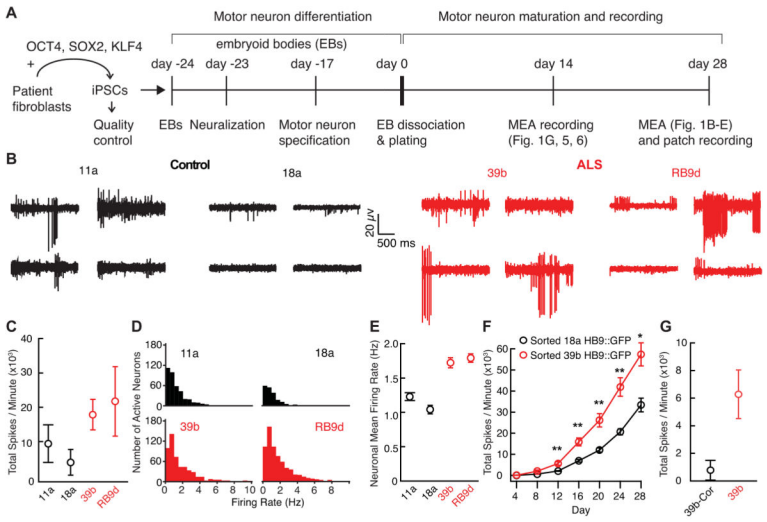

Figure 1. Multi-Electrode Array (MEA) Recording Reveals Increased Spontaneous Firing in ALS-Derived Neurons Compared to Control-Derived Neurons

(A) Schematic of differentiation and recording.

(B) Representative recordings from 4 out of 64 MEA electrodes in control (11a, 18a) and ALS (39b, RB9d)-derived neurons cultured for 28 days on the arrays.

(C) Total action potential firing rate during one minute of recording from MEAs (11a, n=3; 18a, n=3; control mean 6,510 ± 3,131 spikes/minute; 39b, n=3; RB9d, n=3; ALS mean 20,528 ± 5,069 spikes/minute; $p<0.05$, t-test).

(D) Mean firing rate histograms of individual neurons from MEAs in B. See also Figure S1.

(E) Average of mean firing rate for patient-derived neurons (11a, n=381; 18a, n=191; control mean 1.17 ± 0.04 Hz; 39b, n= 520; RB9d, n=662; ALS mean 1.76 ± 0.05 Hz; $p<10^{-15}$, t-test).

(F) Total action potential firing rate during one minute recordings from MEAs of FACS-sorted 18a *Hb9*::GFP and 39b *Hb9*::GFP motor neurons recorded every four days (repeated measures ANOVA F-test $p=1\times10^{-4}$ for difference between lines; post-hoc t-tests with Bonferroni correction for multiple testing indicated as * for $p<0.05$ and ** for $p<0.01$). See also Figures S2–S3.

(G) Total action potential firing rate during one minute of recording from MEAs cultured for 14 days on the arrays (39b-Cor, n=4; mean 775 ± 712 spikes/minute; 39b, n=4; 39b mean 6,278 ± 1,758 spikes/minute; p=0.01, t-test).

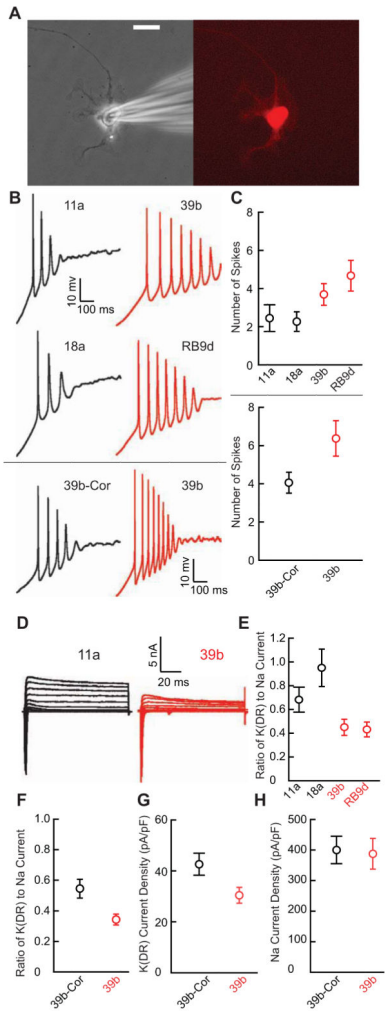

Figure 2. ALS Patient-Derived Motor Neurons are Hyperexcitable and Have Reduced Delayed-Rectifier Potassium Currents Compared to Control-Derived Motor Neurons

(A) An iPSC-derived motor neuron identified by *Hb9*::RFP lentiviral transduction (right) and during patch clamp recording (left) after culture for 28 days. Scale bar 20 μm.

(B) Representative current clamp recordings during ramp depolarization from control and ALS patient-derived motor neurons (upper four panels); sample recordings from separate experiments comparing the isogenic correction of the 39b $SOD1^{A4V}$ mutation (39b-Cor) and 39b (lower two panels).

(C) Upper panel: Average number of action potentials elicited by ramp depolarization from control (11a, n=12; 18a, n=11; control mean 2.5 ± 0.4) and ALS (39b, n=13; RB9d, n=12; ALS mean 4.2 ± 0.5) motor neurons obtained from four separate differentiations ($p<0.05$, Mann-Whitney U test). Lower panel: Separate experiments showing average number of action potentials during ramp depolarization from 39b-Cor (n=17; mean 4.1 ± 0.5) and 39b (n= 19; mean 6.4 ± 0.9) motor neurons from three additional differentiations ($p<0.05$, Mann-Whitney U test).

(D) Sample voltage clamp recordings from control and ALS-derived *Hb9*::RFP-positive motor neurons cultured for 28 days.

(E) Average delayed-rectifier (DR) steady-state potassium current amplitude relative to peak sodium current amplitude in control (11a, n=12; 18a, n=11; control mean 0.88 ± 0.087) and ALS (39b, n=13; RB9d, n=12; ALS mean 0.44 ± 0.054) patient-derived motor neurons from four differentiations ($p<0.001$, t-test).

(F) Experiments from three separate differentiations showing average delayed-rectifier steady-state potassium current amplitude relative to peak sodium current amplitude in 39b-Cor (n=18; mean 0.54 ± 0.061) and 39b (n=19; mean 0.32 ± 0.036; $p<0.005$, t-test).

(G) Direct measurement of delayed-rectifier voltage-gated potassium current isolated by holding at −30 mV, stepping to a test-potential of +40 mV for 2 s and normalizing steady state current amplitude to cell capacitance in 39b-Cor (n=19; mean 42.6 ± 4.3 pA/pF) and 39b (n=18; mean 30.3 ± 3.1 pA/pF; $p<0.05$, t-test) derived motor neurons using cells from two additional separate differentiations.

(H) Peak sodium current amplitude normalized to cell capacitance in 39b-Cor (n=16; mean 400.4 ± 44.7 pA/pF) and 39b (n=15; mean 387.1 ± 50.5 pA/pF; $p=0.8$, t-test) derived motor neurons.

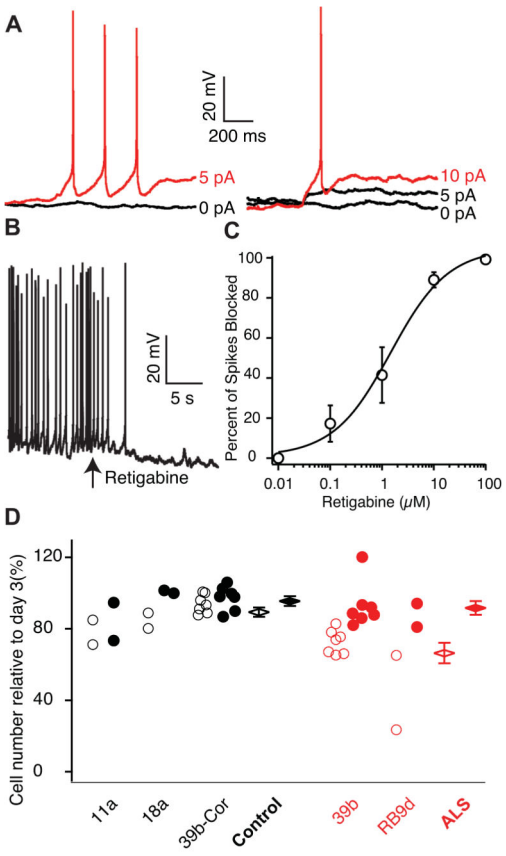

Figure 3. Retigabine Reduces Motor Neuron Excitability and Increases Survival

(A) Rheobase measurements in a 39b *Hb9*::RFP-positive ALS-derived motor neuron in whole-cell patch clamp before (left) and after (right) the application of 10 μM retigabine (baseline rheobase 4.8 ± 1.5 pA vs post-retigabine rheobase 8.4 ± 2.2 pA; n=11; $p<0.05$, Wilcoxon signed rank test).

(B) Representative current clamp recording showing effect of 10 μM retigabine on membrane voltage and spontaneous firing (baseline Vm −60.4 ± 2.9 mV vs post-retigabine Vm −66.3 ± 3.6 mV, n=11; p=0.001, t-test). In (A–B), CNQX (15 μM), D-AP5 (20 μM), bicuculline (25 μM), and strychnine (2.5 μM) were added to the external solution.

(C) Dose response curve for retigabine on suppression of spontaneous action potentials in MEA recording and Hill plot fit of mean data from 39b (n=4) and RB9d (n=4) with EC50 1.5 ± 0.8 μM.

(D) Effect of vehicle (open circles) and 1μM retigabine (filled circles) treatment from days 14–28 of culture on the survival of Islet-positive, Tuj1-positive motor neurons measured at day 30 (total control n=11; total ALS n=9; F-test for effect of retigabine on all cells $p=3.8\times10^{-4}$; effect of retigabine in ALS motor neurons, red, 25.3% (SD 5.6; t-test $p=6.4\times10^{-5}$); effect of retigabine in control motor neurons, black, 6.1% (SD 5.1, p=0.23). Cell counts are from individual wells for four separate differentiations. See also Figure S4.

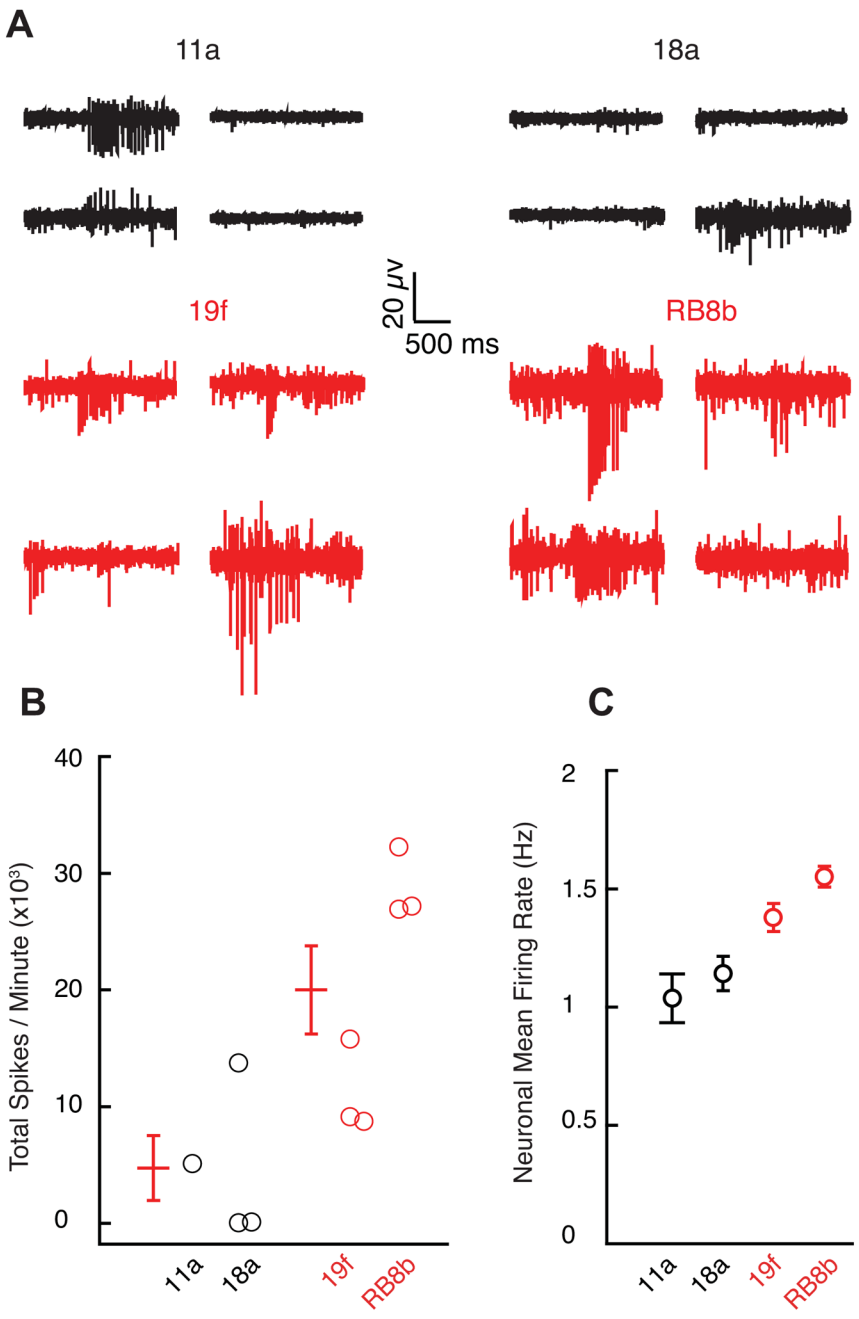

Figure 4. Hyperexcitability of *C9orf72* Repeat Expansion-Derived Motor Neurons

(A)Representative recordings from four/64 MEA electrodes recorded from control (11a, 18a) and *C9orf72* expansion ALS-derived neurons (19f, RB8b) cultured for 14 days.

(B) Total action potential firing rate during one minute of recording from MEAs (11a, n=1; 18a, n=3; control mean 4,752 ± 2,786 spikes/minute; 19f, n=3; RB8b, n=3; ALS mean 20,022 ± 3,775 spikes/minute; $p<0.05$, t-test).

(C) Average of mean firing rate for control and *C9orf72*-derived neurons (11a, n=82; 18a, n=203; control mean 1.11 ± 0.06 Hz; 19f, n=407; RB9d, n=929; ALS mean 1.50 ± 0.04; $p<10^{-5}$, t-test).

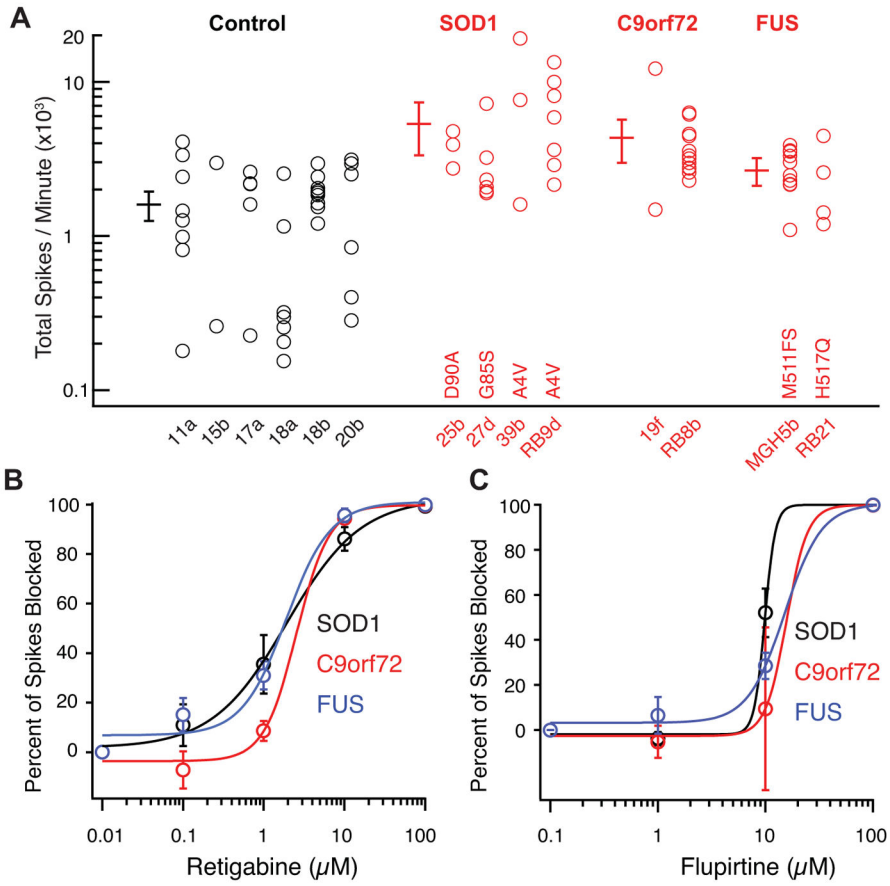

Figure 5. Motor Neuron Hyperexcitability and Block by Retigabine are Broad Properties of ALS Variants

(A) Multi-electrode array recordings of motor neurons derived from control (11a, n=8; 15b, n=2; 17a, n=5; 18a, n=7; 18b, n=10; 20b, n=6), *SOD1* (25b, D90A, n=3; 27d, G85S, n=7; 39b, A4V, n=3; RB9d, A4V, n=7), *C9orf72* expansion (19f, n=2; RB8B, n=13) and *FUS* (MGH5b, frameshift mutation at residue 511, n=10; RB21, H517Q, n=4) subjects cultured for 14 days. ANOVA, $p < 10^{-7}$; Tukey's post-hoc tests for control vs *SOD1* $p<0.01$, control vs *C9orf72* $p<0.01$, control vs *FUS* $p<0.05$. For subject 18, motor neurons from two different iPSC lines were recorded. Error bars are 95% CI. See also Figure S5.

(B) Dose response curve for retigabine on suppression of spontaneous action potentials in MEA recording and Hill plot fit of mean data from *SOD1* (n=10; EC50 1.9 ± 0.5 μM), *C9orf72* (n=9; EC50 2.6 ± 0.8 μM) and *FUS* (n=4; EC50 1.9 ± 1.1 μM).

(C) Dose response curve for flupirtine on suppression of spontaneous action potentials in MEA recording and Hill plot fit of mean data from *SOD1* (n=5; EC50 9.8 μM), *C9orf72* (n=4; EC50 19.4 μM) and *FUS* (n=2; EC50 15 μM).